Rock and Soil Mechanics 2025 46(3): 930−942 ISSN 1000−7598
https: //doi.org/10.26599/RSM.2024.94300554 journal homepage: rocksoilmech.whrsm.ac.cn

Calculation method of negative skin friction for end-bearing piles based on soil deformation

ZHOU Guang-yuan[1], GAN Fei[1, 2], ZHENG Gang[2], ZHOU Hai-zuo[2], WANG Hong[1], BI Jing[1], LIU Biao[3], ZHANG Yuan-yin[3]

1. School of Civil Engineering, Guizhou University, Guiyang, Guizhou 550025, China
2. School of Architectural Engineering, Tianjin University, Tianjin 300072, China
3. Guizhou Power Transmission and Transformer Company Limited, Guiyang, Guizhou 550000, China

Abstract: The application of a significant additional load induces soil deformation around the pile, generating a downward drag force, commonly referred to as negative skin friction. This phenomenon significantly reduces the pile's ultimate axial load capacity. Therefore, precise estimation of negative skin friction is crucial for pile design. To accurately calculate the negative skin friction acting on the pile, it is essential to determine the stress states at the pile-soil interface under varying soil deformations. However, many existing methodologies solely consider peak or residual stresses on the shear plane, neglecting the process of stress changes in soil deformation. This approach often results in an overestimation of negative skin friction. In this investigation, we propose a novel method for calculating negative skin friction that comprehensively accounts for the whole process of stress state alterations occurring during soil deformation (pre-failure zone and peak stress, post-failure zone and residual stress state) and describes the relationship between soil deformation and stress using a hyperbolic mechanical model. On this basis, soil deformation behavior is classified into three distinct forms. The spatial distribution characteristics for negative skin friction were then explored individually for each form. Additionally, the influence of different soil parameters on the spatial distribution of negative skin friction was also investigated. Finally, the accuracy and applicability of the new negative skin friction calculation method is validated through comparison with field measurement data. It can be used as a reference for practical engineering.

Keywords: soil deformation; negative skin friction; pile foundation; stress state; hyperbolic mechanical model

1 Introduction

A fundamental role of pile foundations is to support vertical loads[1]. However, when large-scale surcharge pressure is applied at the ground surface[2], The deformation of the soil will be more significant than the pile deformation, leading to negative skin friction (NSF) acting laterally on the pile. Drag loads induced by NSF diminish the vertical bearing capacity of pile foundations. NSF is a crucial factor in pile design, and the key to accurately predicting NSF is to obtain the state of stress on the pile-soil contact surface under different soil deformations.

Predicting the NSF on the pile side is a complex problem. While accurate results can be obtained through in situ experiments in the field[3−6] and laboratory tests[7−10], these methods are often costly and challenging to implement. Therefore, numerous theoretical calculations have been proposed to streamline this process. For instance, Terzaghi et al[11] introduced the initial method to calculate NSF, yet this conventional approach neglects soil deformation around the pile from surcharge pressure. Kong et al.[12] proposed a simple calculation method for NSF under consideration of surcharge pressure but did not consider the change of stress state of the complete soil deformation process. Zhao et al.[13−14] established a method for calculating NSF based on the pile body's energy balance and static balance equations by considering soil deformation under concentrated load. However, the method is complicated to calculate, and in practical engineering applications, the ground load is mainly distributed load, so the method is not applicable. Seed et al[15] proposed a load transfer method that clarifies the relationship between relative pile-soil displacement and soil friction. Numerous scholars have established NSF calculation methods on this basis[16−18]. Despite the mathematical simplicity of the load transfer method, it oversimplifies the mechanical behaviour of the soil[19]. This method does not consider the progressive failure process of the soil mass and fails to calculate the magnitude of critical deformation, thus being unable to accurately determine the stress variation along the pile-soil shear interface.

Soil deformation is a progressive failure process[20], and there are significant differences in the degree of failure exhibited by pile periphery soil located at different

Received:2024-08-25 Accepted: 2024-10-14
The research was supported by the National Natural Science Foundation of China (52164001) and the Science and Technology Support Plan Foundation of Guizhou Province ([2021]–general511).
First author: ZHOU Guang-yuan, male, born in 2000, MA, mainly engaged in pile foundation and slope stability research. E-mail: 13416330651@163.com
Corresponding author: GAN Fei, male, born in 1987, PhD, Associate Professor, mainly engaged in teaching and research in geotechnics.
E-mail: fgan@gzu.edu.cn

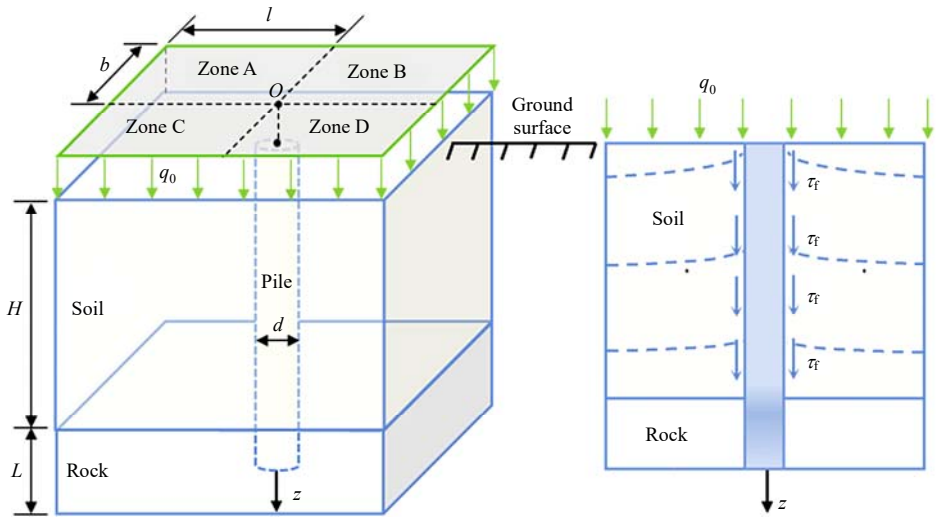
depths. These differences further lead to a heterogeneous distribution of stress states characterizing the pile-soil contact interface. Some regions may be in a pre-failure stress state, while others may have reached a peak stress state or be in a post-failure stress state[21−22]. In the existing literature, the strength criterion usually adopted for predicting NSF mainly focuses on considering peak or residual stresses on the pile-soil contact surface[23−24] and tends to ignore the non-linear relationship between shear stress and deformation. Gan et al.[21, 25−26] did a large number of experiments and established a hyperbolic mechanical model, which accurately describes the shear stress–strain non-linear relationship on the pile-soil contact surface.

We are trying to calculate the NSF of the piles more accurately to provide practical help for pile design and avoid unnecessary waste. In this study, the Boussinesq stress solution stratified sum method is used to calculate the soil deformation caused by surcharge pressure, and a hyperbolic mechanical model is introduced to describe the stress–strain relationship between the pile-soil contact surface to establish a simple and effective method for calculating NSF. Based on this, the soil deformation was classified into three different forms, and the spatial distribution characteristics of the NSF under the three forms were investigated separately. Furthermore, the impacts of varying soil cohesion and internal friction angle on the spatial distribution of NSF were also studied. Finally, known field tests are used to verify the accuracy of the calculation methods in this paper.

2 Theoretical framework

2.1 Pile-soil system and basic assumptions

This investigation proposes a new approach for civil engineers to estimate the NSF of a single pile under surcharge pressure. Fig. 1 shows a sketch of the pile-soil system. Frictional resistance in the pile body is influenced by the extent of relative pile-soil displacement, escalating as this displacement grows until it hits a maximum threshold. Given the pile's significantly higher compressive modulus than the soil[27−28], this study exclusively considers soil deformation. The soil around the pile is usually subjected to distributed loads, and the settlement difference along the effective settlement radius is slight[19]. Under distributed loads, the stress state of the soil body changes, which is the leading cause of soil deformation[29]. Soils exhibit progressive failure, appearing as a non-linear relationship between shear stress and deformation at the contact surface. As shown in Fig. 2, where τ_{peak} is the peak shear stress; τ_{resid} is the residual shear stress; v_{crit} is the critical deformation; and v_{resid} is the residual deformation. A point on the pile-soil interface will be in different stress states (pre-failure zone and peak stress, post-failure zone and residual stress state) at different times. The points on the pile-soil contact surface simultaneously are not likely to be in the same stress state, and all points in a peak stress state do not exist[21]. Based on this, the following assumptions need to be considered during the derivation of the NSF calculation method:



(a) before deformation (b) after deformation

Fig. 1 Pile-soil system

(1) The soil layer is an isotropic homogeneous elastic semi-infinite medium.

(2) The end bearing pile body is vertical and rigid. Under external loading, only the deformation of the soil body is considered while the deformation of the pile body and the rock at the pile end is ignored.

(3) The soil around the pile is subjected to surcharge pressure as a distributed load and only produces vertical deformation without lateral expansion deformation.

(4) The additional stress at the pile foundation's

center represents the value of the additional stress in the surrounding soil.

(5) The stress–strain relationship of the soil around the pile satisfies the hyperbolic mechanics model:

$$\tau = \mathrm{e}^{-\zeta v^{\lambda}}\, c\rho(\lambda\zeta\mathrm{e})^{\frac{1}{\lambda}} v + (1-\mathrm{e}^{-\zeta v^{\lambda}})\sigma_{\mathrm{n}} \tan\varphi \tag{1}$$

Where τ is the shear stress at the pile-soil interface (kPa); v is the shear deformation (mm); λ is a dimensionless coefficient related to the cohesive force and friction force; ζ is a parameter primarily associated with the velocity of change and the plasticity of the cohesive medium ($\mathrm{mm}^{-\lambda}$); e is the natural constant; σ_{n} is the normal stress on the pile-soil contact surface (kPa); φ is the residual internal friction angle of the shear surface (°); ρ is the positive pressure influence function.

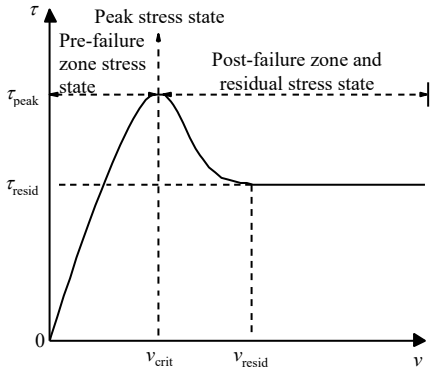


Fig. 2 Stress-deformation relationship curve of the pile-soil contact surface

2.2 Establishing the NSF calculation equation

2.2.1 Soil deformation

There are many ways of obtaining soil deformation, either by fitting it to actual measurements or by calculating it according to the layering method of elasticity theory[30]. In practice, soils are usually well consolidated under self-weight, such that the surcharge pressure at the ground and the self-weight of the newly filled soils are the driving factors for soil deformation. Therefore, the effect of surcharge pressure should be considered, and the impact of the soil's weight should be ignored[31−32]. Many scholars have used the Boussinesq stress solution hierarchical summation method to calculate soil deformation due to surcharge pressure under the bearing platform[33−34]. As shown in Fig. 1(a), the soil deforms under surcharge pressure q_0, here, H is the thickness of the soil layer (m); L is the embedded length of the pile into the rock mass (m); and d is the diameter of the pile (m). Divide the surcharge pressure into four equal-sized zones (zone A, zone B, zone C and zone D). For zone A, its additional stress along the y-axis at the corner point O can be calculated from the following equation:

$$\left.\begin{aligned} \sigma_z &= \alpha_{\mathrm{c}}(z) q_0 \\ \alpha_{\mathrm{c}}(z) &= \frac{lbz(l^2+b^2+2z^2)}{2\pi(l^2+z^2)(b^2+z^2)\sqrt{l^2+b^2+z^2}} + \\ &\quad \frac{\arctan\dfrac{lb}{z\sqrt{(l^2+b^2+z^2)}}}{2\pi} \end{aligned}\right\} \tag{2}$$

Where σ_z is the additional stress (kPa); $\alpha_{\mathrm{c}}(z)$ is the coefficient of vertical additional stress at the corners of the rectangle; z is the depth (m); l and b are the length and width (m) of the rectangle, respectively. The additional stresses in the soil on the side of the pile are the algebraic superposition of the additional stresses in the four zones A, B, C, and D at the corner point O. Since the four zones have the same area and side lengths, the additional stress in the soil at depth z is calculated by the following equation:

$$\sigma_z(z) = \frac{2q_0}{\pi}\left[\frac{lbz(l^2+b^2+2z^2)}{(l^2+z^2)(b^2+z^2)\sqrt{l^2+b^2+z^2}} + \arctan\frac{lb}{z\sqrt{l^2+b^2+z^2}}\right] \tag{3}$$

This paper uses the layered sum method to calculate soil deformation[27, 35]. The layered sum method assumes the soil is a linear deformation body. The deformation generated under the action of the external load occurs only in the compression layer. The compression layer will be divided into a number of layers of soil to determine the stress of each layer of the soil body, according to the stress–strain relationship equation of the soil, and to calculate the amount of deformation of each layer. This aligns with the requirements of the *Technical Code for Piling of Chinese Buildings* (JGJ 94—2008)[36]. As shown in Fig. 3, the soil layer is divided into n layers and the deformation of each layer is calculated. Layered summation method equations are:

$$\left.\begin{aligned} v_i &= \frac{\bar{\sigma}_{zi} h_i}{E_{si}} \\ v &= \sum_{i=1}^{n} v_i \end{aligned}\right\} \tag{4}$$

Where v_i is the deformation of the i-th layer soil; E_{si} is the compression modulus of the soil in layer i-th, $\bar{\sigma}_{zi}$ is the average additional stress of the soil in layer i-th, and h_i is the thickness of the soil in layer i-th. $\bar{\sigma}_{zi} h_i$ is equal to the area enclosed by the additional stress curve of the soil in layer i-th, which the following equation can calculate:

$$\bar{\sigma}_{zi} h_i = A = \int_{z_{i-1}}^{z_i} \sigma_z \mathrm{d}z \tag{5}$$

Where A is the area enclosed by the additional stress curve;

z_i and z_{i-1} are the depths (m) of the *i*-th and *i*-1 layer soil, respectively.

Substituting Eqs. (5) into the first equation of Eq. (4) yields the deformation of layer *i*-th soil:

$$v(h)=\int_0^h \frac{2q_0\left[\dfrac{lbz(l^2+b^2+2z^2)}{(l^2+z^2)(b^2+z^2)\sqrt{l^2+b^2+z^2}}+\arctan\dfrac{lb}{z\sqrt{l^2+b^2+z^2}}\right]}{\pi E_{si}}\mathrm{d}z \tag{7}$$

Where *h* is the effective calculated depth (m) of negative skin friction.

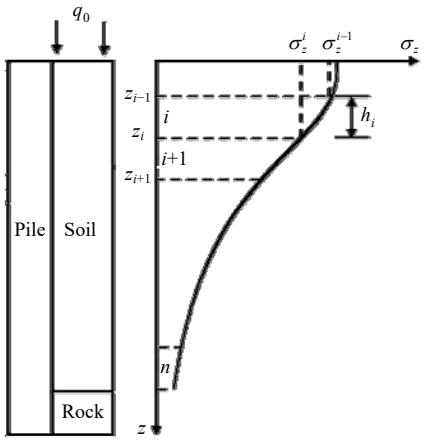


Fig. 3 Layered sum method calculation sketch

2.2.2 Negative skin friction (NSF)

As shown in Fig. 1(b), due to the deformation of the soil, a downward friction stress τ_f is exerted on the pile body. Gan et al.[21, 25−26] introduced a pair of exponential alternating transition functions to describe the conversion process of friction and cohesion on the shear surface based on the Mohr-Coulomb strength criterion, considered the effect of normal stress on the bond strength, and established a hyperbolic mechanical model. The model can describe most mechanical behaviours in geotechnical materials, such as elastic-brittle, ideal elastoplastic, elastoplastic hardening, and elastoplastic softening characteristics. It also accurately reflects the strain softening in the material's post-failure region. The hyperbolic mechanical model equations are as follows:

$$\tau=\mathrm{e}^{-\zeta v^{\lambda}}c\rho(\lambda\zeta\mathrm{e})^{\frac{1}{\lambda}}v+(1-\mathrm{e}^{-\zeta v^{\lambda}})\sigma_{\mathrm{n}}\tan\varphi \tag{8}$$

$$G=c\rho(\lambda\zeta\mathrm{e})^{\frac{1}{\lambda}} \tag{9}$$

$$\rho=1+\kappa(1-\mathrm{e}^{-\chi\sigma_{\mathrm{n}}}) \tag{10}$$

Where *c* is the cohesive force on the shear plane (kPa); *G* is the unit shear modulus of the cohesive force part (kPa/mm); κ is a dimensionless influence parameter determining the maximum degree to which normal stress affects cohesive force; χ is a coefficient related to the rate at which normal stress affects the cohesion force

$$v_i=\frac{1}{E_{si}}\int_{z_{i-1}}^{z_i}\sigma_z(z)\mathrm{d}z \tag{6}$$

Then, the overall deformation of the soil can be calculated by the following equation:

(1/kPa).

To unify the units in Eq. (8), (9), (10), Gan et al.[21, 25−26] stipulate the unit of the unit tangent modulus *G* is kPa/mm, and the unit of parameter ζ is $\mathrm{mm}^{-\lambda}$, which makes the units in the formula complicated. Replace the shear deformation *v* in the formula with the dimensionless shear strain ε to simplify the dimension of the formula. The improved formula is as follows:

$$\left.\begin{aligned}&\tau=\mathrm{e}^{-\zeta\varepsilon^{\lambda}}c\rho(\zeta\lambda\mathrm{e})^{\frac{1}{\lambda}}\varepsilon+(1-\mathrm{e}^{-\zeta\varepsilon^{\lambda}})\sigma_{\mathrm{n}}\tan\varphi\\&G=c\rho(\zeta\lambda\mathrm{e})^{\frac{1}{\lambda}}\\&\rho=1+\kappa(1-\mathrm{e}^{-\chi\sigma_{\mathrm{n}}})\end{aligned}\right\} \tag{11}$$

Where the parameter ζ is a dimensionless coefficient, and its meaning is consistent with parameter ζ in Eq. (1), both primarily associated with the rate of change and the plasticity of the cohesive medium. However, unlike previous numerical values, it requires a new value assignment in this context. The method of taking the value of the parameters ζ, λ, κ, χ is described in the literature [25].

The improved hyperbolic mechanical model needs to obtain the shear strain at any point of the soil to calculate the friction resistance.

The strain at point z_0 can be derived from the following equation:

$$\varepsilon=\frac{\sigma_z(z_0)}{E_{si}} \tag{12}$$

Substituting Eq. (12) into Eq. (11) yields the Eq. (13) for calculating the NSF at any point of the pile body:

$$\left.\begin{aligned}&\tau_{\mathrm{f}}=\mathrm{e}^{-\zeta\varepsilon^{\lambda}}c\rho(\zeta\lambda\mathrm{e})^{\frac{1}{\lambda}}\varepsilon+(1-\mathrm{e}^{-\zeta\varepsilon^{\lambda}})\sigma_{\mathrm{n}}\tan\varphi\\&G=c\rho(\zeta\lambda\mathrm{e})^{\frac{1}{\lambda}}\\&\rho=1+\kappa(1-\mathrm{e}^{-\chi\sigma_{\mathrm{n}}})\\&\sigma_{\mathrm{n}}=(\gamma z+\sigma_z)k_0\\&\varepsilon=\frac{2q_0}{\pi E_{si}}\left[\frac{lbz(l^2+b^2+2z^2)}{(l^2+z^2)(b^2+z^2)\sqrt{l^2+b^2+z}}+\right.\\&\qquad\left.\arctan\frac{lb}{z\sqrt{l^2+b^2+z}}\right]\end{aligned}\right\} \tag{13}$$

Where γ is the unit weight (kN/m³); k_0 is the static soil pressure coefficient, $k_0 = 1-\sin\varphi$.

2.2.3 Drag load

The drag load is the sum of the NSF above the neutral point of the pile[37−38]Based on the NSF formula in this paper, the formula for the drag load can be derived:

$$Q_n = \pi d \frac{h}{n}\sum_{i=1}^{n}\tau_f \tag{14}$$

2.2.4 Calculation process

The flowchart of negative skin friction calculation is shown in Fig. 4. The calculation process includes the following steps: firstly, calculate the additional stress caused by the surcharge pressure; secondly, calculate the deformation of the soil and the normal stress acting on the pile-soil interface; thirdly, obtain the necessary parameters (ζ, λ, κ, χ) of the hyperbolic mechanical model from the straight shear test; and finally, calculate the NSF and the drag load of the pile. To improve the calculation speed and accuracy, we used Matlab programming for the calculation.

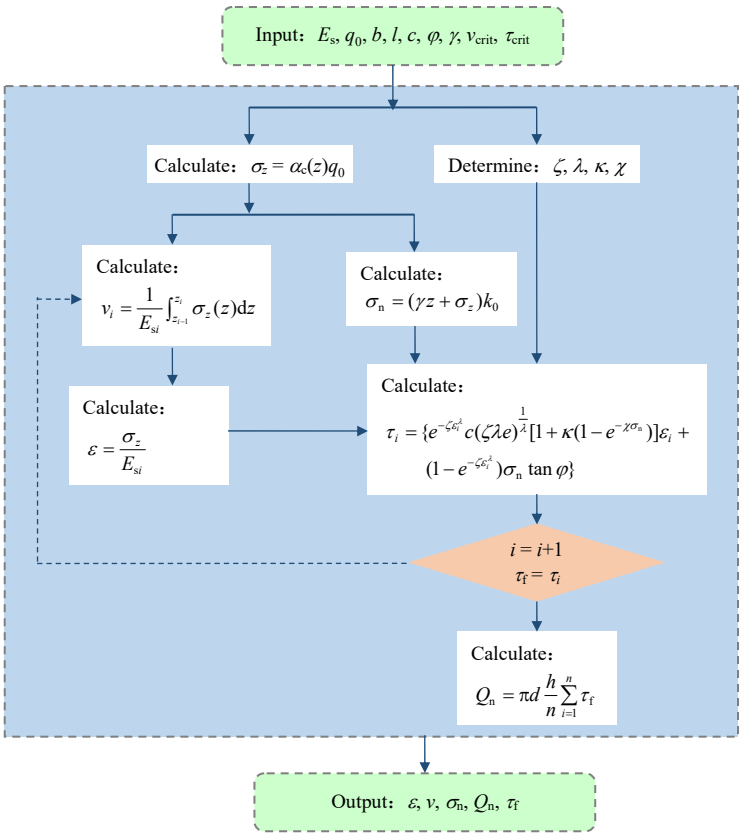


Fig. 4 Calculation flow chart

3 Analyze the spatial distribution of NSF

In order to investigate the spatial distribution of negative skin friction (NSF) along the pile and facilitate the calculation, it is assumed that the soil around the pile is a homogeneous, isotropic, semi-infinite body. We have simplified the parameters of the hyperbolic mechanical model describing the mechanical properties of the soil around the piles (ζ = 1 000, λ = 1.0, κ = 1.0, χ = 1.0 kPa^{-1}). As shown in Fig. 5, the depth of the pile L buried in the soil part is 15 m; the diameter of the pile is 1 m; the surcharge pressure is a homogeneous rectangular load of 6 m×6 m. The soil layer was divided into n layers, each 100 mm thick, and the deformation of each layer, as well as the NSF of the pile, was calculated using Matlab programming.

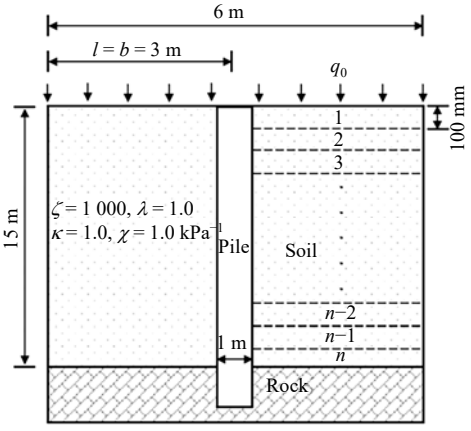


Fig. 5 Computational modelling diagram

3.1 Influence of soil deformation

With the development of soil deformation around the pile, the corresponding pile-soil contact surface stress changes, and the pile-soil contact surface at any point will experience the stress–strain characteristics of the whole process, that is, in the pre-failure zone, the peak stress, post-failure zone, the residual stress of the four states. This section explores the spatial distribution of NSF along the pile in three forms, depending on the degree of soil failure. The Form I for the soil body has not occurred failure; the entire contact surface is in the pre-failure zone stress state. The Form II is that part of the soil undergoes failure; the whole contact surface is partly under stress in the pre-failure zone, partly under peak stress, and partly under the post-failure zone and residual stress state. The Form III is that the whole soil is damaged; the entire contact surface is in the post-failure zone and residual stress state. In this section, the critical deformation discussed refers specifically to the critical deformation values at various points in the soil around the pile. In order to study the spatial distribution of negative skin friction, the hyperbolic mechanical model parameters are simplified, which may lead to the calculated critical deformation being smaller than the actual value(1−3 mm)[39−40]. Therefore, the model parameters need to be adjusted according to the field data to ensure that they are consistent with the actual situation.

3.1.1 Form I

When the surcharge pressure on the ground surface is 8 kPa, the soil deformation is minimal and shows a non-linear decrease along the pile. The maximum deformation of the soil occurs in soil layer a, and its deformation value is equal to the critical deformation v_{crit}. In contrast, the deformation of the remaining soil layers is less than the critical deformation (Fig. 6(a)).

Due to the progressive failure characteristics of the soil, the same layer of soil will change its stress state on the contact surface with the pile as the deformation develops. Four soil layers at different depths were selected (a, b, c, d). Each soil layer has a different degree of failure, and its corresponding stress state on the pile-soil contact surface is also different. Fig. 6(b) shows the soil deformation versus stress curves for layers a, b, c, and d. *a′*, *b′*, *c′*, and *d′* correspond to the stress state of the soil in layers a, b, c, and d, respectively, at the time of reaching the final deformation. It can be seen that when the deformation of soil in layer a develops to the critical deformation, the stress at the pile-soil contact surface is in the peak stress state (*a′*), and since the deformation of soil in the remaining layers is ultimately more minor than the critical deformation, the pile-soil contact surface is all in the stress state before the peak stress, that is, the pre-failure zone stress state.

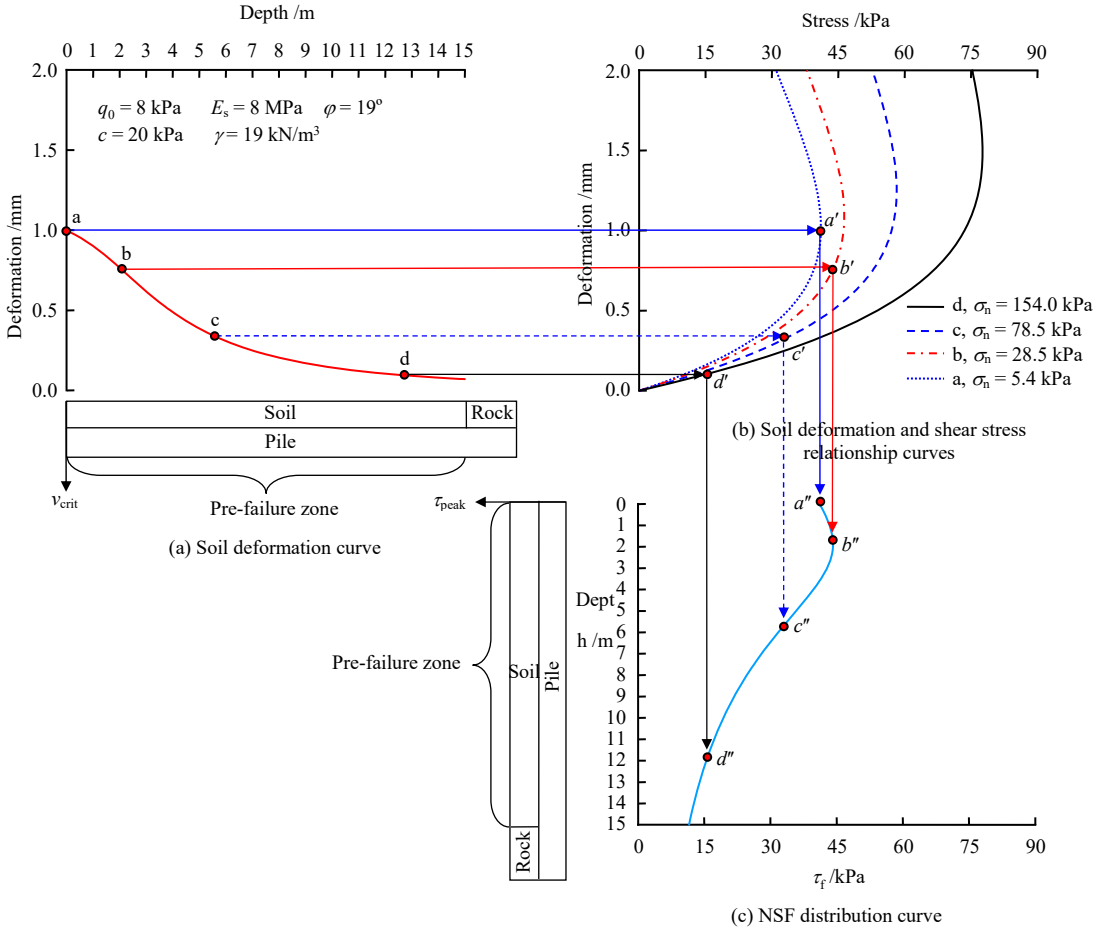


Fig. 6 Form I

Fig. 6(c) shows the spatial distribution of NSF along the pile when the entire pile-soil contact surface is in the pre-failure zone. The *a″*, *b″*, *c″*, and *d″* correspond to the negative skin friction (NSF) of the pile at the time of reaching the final deformation of the soil in layers a, b, c, and d, respectively. NSF shows a non-linear distribution along the pile, which increases first and then decreases. NSF is affected by normal stress and soil deformation together. In the 0−2 m interval, the soil deformation is significant, but the normal stress is low, and the NSF increases mainly with the increase of normal stress. While in the interval 2−15 m, the normal stresses are high enough to mobilize the resistance on the contact surface, the NSF shows a decreasing trend due to the reduction of soil deformation.

3.1.2 Form II

The surcharge pressure is raised to 90 kPa, and Fig. 7(a) shows the distribution curve of soil deformation along the pile. The curve indicates that the soil deformation in the range of 0−10 m has exceeded the critical deformation, the cementing material of this part of the soil has been damaged, and the pile-soil contact surface is in the post-failure zone and residual stress state. The soil deformation at 10 m is at critical deformation, and this part of the pile-soil contact surface is at peak stress. The soil deformation in the 10−15 m range is less than the critical deformation, the soil is not damaged, and the pile-soil contact surface is in the pre-failure stress state.

Four soil layers at different depths were selected (a, b, c, d). Each soil layer has different degrees of failure, and its corresponding stress state on the pile-soil contact surface is also different. Fig. 7(b) shows the deformation versus stress curves for layers a, b, c, and d of the soil. With the development of soil deformation, the stress at the pile-soil contact surface shows a change characteristic of first increasing and then decreasing, and finally tends to a constant value. The *a′*, *b′*, *c′*, and *d′* correspond to the state of stress in the a, b, c, and d layers of the soil as it reaches final deformation, respectively. The soil deformation in layer a eventually developed to 10.5 mm, which is in the state of residual stress; the soil deformation in layer b eventually developed to 3.5 mm, which is in the state of post-failure zone stress; the soil deformation in layer c eventually developed to 1.5 mm, which is in the state of peak stress; and the soil deformation in layer d eventually developed to 0.9 mm which is in the state of pre-failure zone stress.

Fig. 7(c) shows the spatial distribution curve of NSF along the pile. The *a″*, *b″*, *c″*, and *d″* correspond to the NSF of the pile at the time of reaching the final

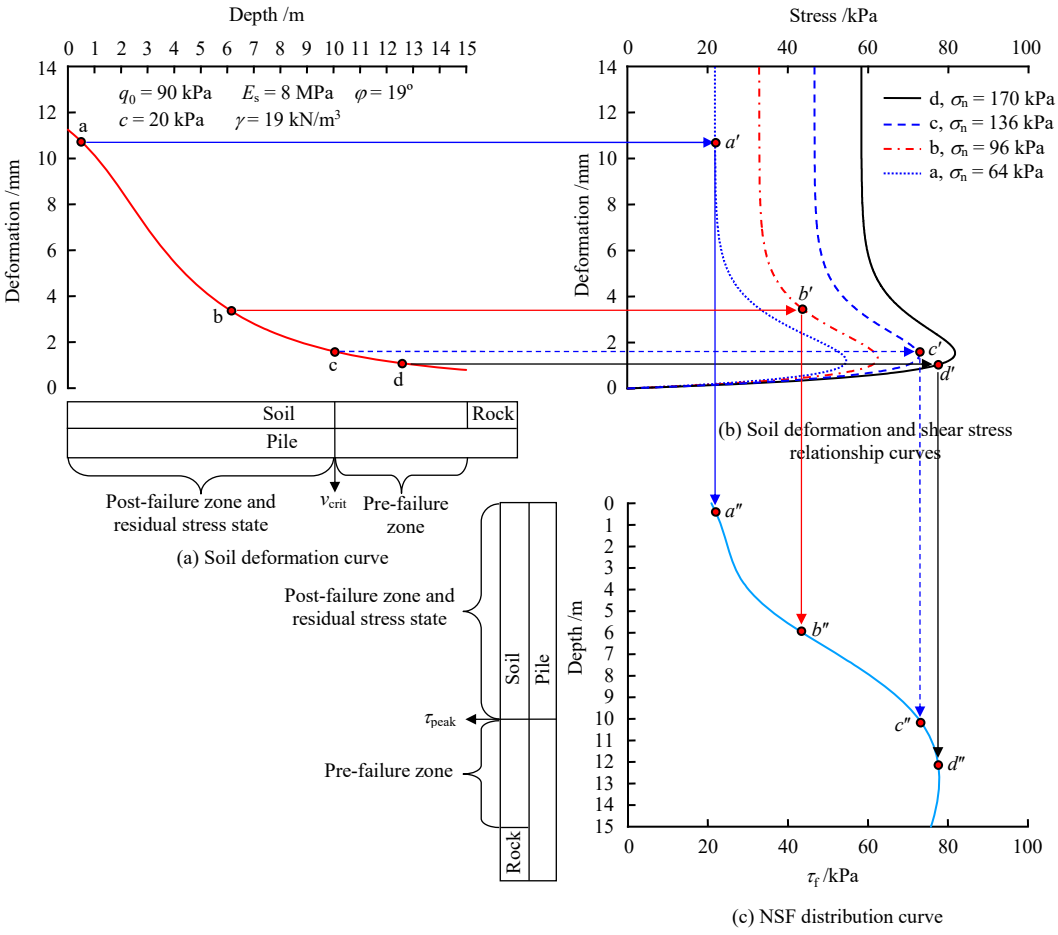


Fig. 7 Form II

deformation of the soil in layers a, b, c, and d, respectively. NSF shows a characteristic change of increasing and then decreasing. In the 0−4 m interval, the soil deformation is significant, so the soil cementing material has been damaged, and the contact surface is in a residual stress state. At this point, the NSF is mainly determined by the normal stress and rises gradually with the growth of the normal stress. The soil deformation was reduced in the 4−10 m range, and the cementing material was not destroyed. The contact surface is in the post-failure zone stress state, and the NSF is affected by the combined effect of soil deformation and normal stress, showing a rapid increase in the change characteristics. In the 10−15 m range, the soil deformation is below the critical value, and the contact surface is in the pre-failure zone stress state. At this time, the NSF is mainly affected by the soil deformation; with the reduction of deformation, the NSF increases slowly and then decreases gradually.

3.1.3 Form III

Raise the surcharge pressure to 180 kPa. The soil deformation shows a non-linear decrease along the pile. The minimum deformation of soil is the deformation value of soil layer d, equal to the critical deformation (v_{crit}), and the deformation of the rest of the soil layers is more significant than the critical deformation. The soil around the pile was damaged, and the entire pile-soil contact surface was in the post-failure zone and residual stress state (Fig. 8(a)).

Four soil layers at different depths were selected (a, b, c, d). Each soil layer has a different degree of failure, and its corresponding stress state on the pile-soil contact surface is also different. Fig. 8(b) shows the deformation versus stress curves for layers a, b, c, and d of the soil. The deformation of the soil in layer d eventually develops into critical deformation. The stress on the contact surface is eventually in the peak stress state, while the final deformation of the rest of the soil layers is larger than the critical deformation. The contact surfaces are all in the post-failure zone and the residual stress state. It is worth noting that the normal stresses in the a-layer soil are greater than those in the b-layer soil, which is caused by the more significant surcharge pressure. In the initial stage, the normal stress increases slowly because the decrease in additional stress is smaller than the increase in soil gravity stress. When the reduction in additional stress exceeds the rise in soil gravity stress, the normal stress begins to decrease slowly. At deeper locations, the normal stresses increase mainly with the rise in soil self-gravitational stresses due to a significant reduction in additional stresses.

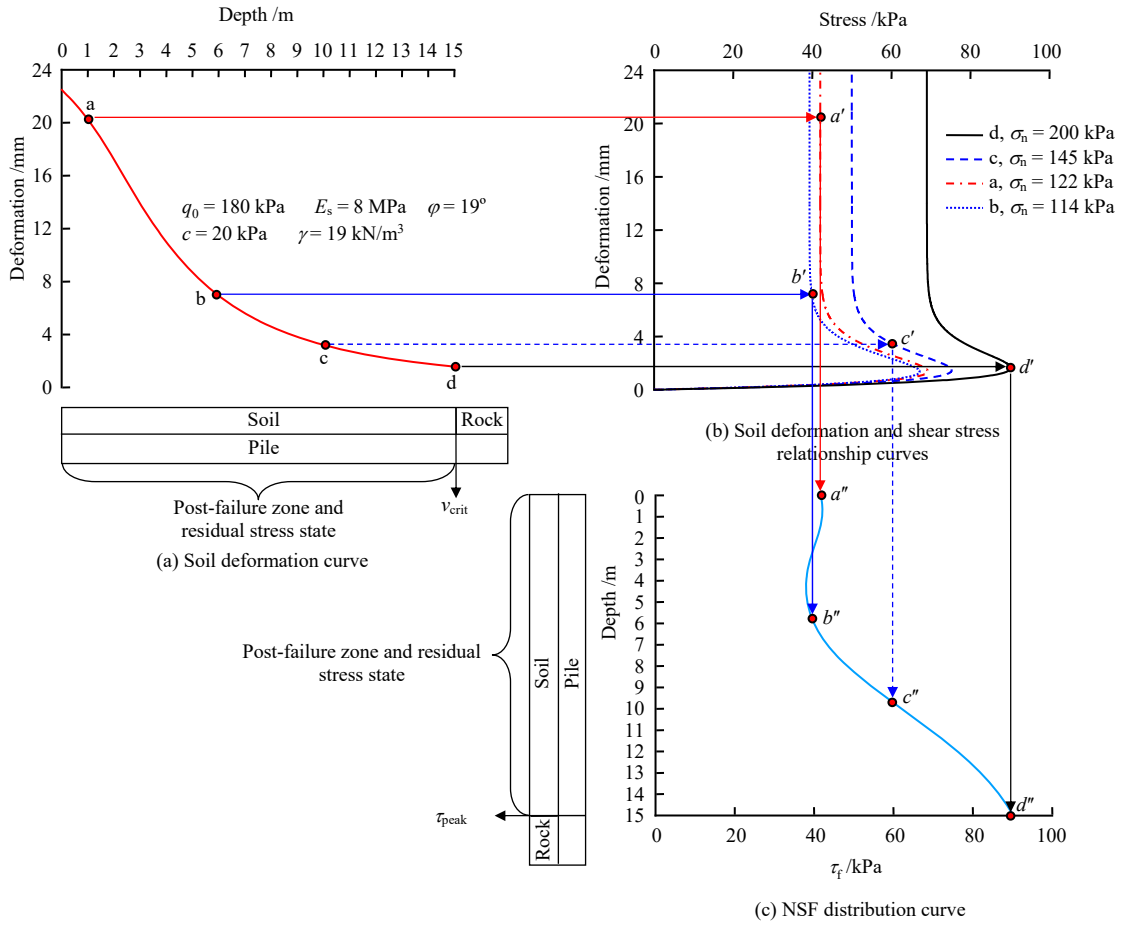


Fig. 8 Form III

Fig. 8(c) shows the spatial distribution curve of NSF along the pile, and the NSF shows the change characteristics of slight decrease and then rapid increase. In the range of 0−6 m, the soil deformation is too large, the soil cementing material is destroyed, the contact surface is in the stage of residual stress, and the NSF is entirely affected by the normal stress, which shows a trend of slight decrease followed by a slow increase. In the 6−15 m range, the soil deformation is small, the soil cementing material is not destroyed, and the NSF is affected by the soil deformation and normal stress together, showing a nearly linear growth trend.

3.2 Influence of soil parameters

The amount of cohesion and internal friction angle of the soil will directly affect the distribution of NSF. In this section, the cohesion is varied from 0 to 30 kPa, and the internal friction angle is varied from 10° to 40° to investigate the effect of cohesion and internal friction angle on NSF, respectively. In monopile mode, the pile length is 15 m, and the pile diameter is 1 m. Soil parameters: E_s = 8 MPa, γ = 19 kN/m^3. Surcharge pressure parameters: $b = l$ = 6 m, q_0 = 60 kPa.

Fig. 9(a) and Fig. 9(b) show that increasing the soil cohesion causes the critical deformations to preat depth meaning the soil layers at the pile-soil interface experiencing peak stress state (a', b', c', d') are now situated at deeper situation. Near the ground surface (depth<3 m), the effect of soil cohesion on the distribution of NSF is insignificant. Still, at deeper locations (depth>3 m), increasing soil cohesion, the NSF of the pile body rises exponentially. It should be noted that for soils with zero cohesion, tiny deformations can put the pile-soil contact surface stresses in a residual stress state.

Fig. 9(c) and Fig. 9(d) show that increasing the soil internal friction angle results in a shallower location of critical deformation (as shown in a', b', c', and d'), i.e., the extent to which the pile-soil contact surface is in the post-failure zone and the residual stress state is reduced. Meanwhile, increasing the soil internal friction angle will not change the distribution characteristics of NSF along the pile, but it will increase NSF. Specifically, the rise in NSF is positively correlated with the increase

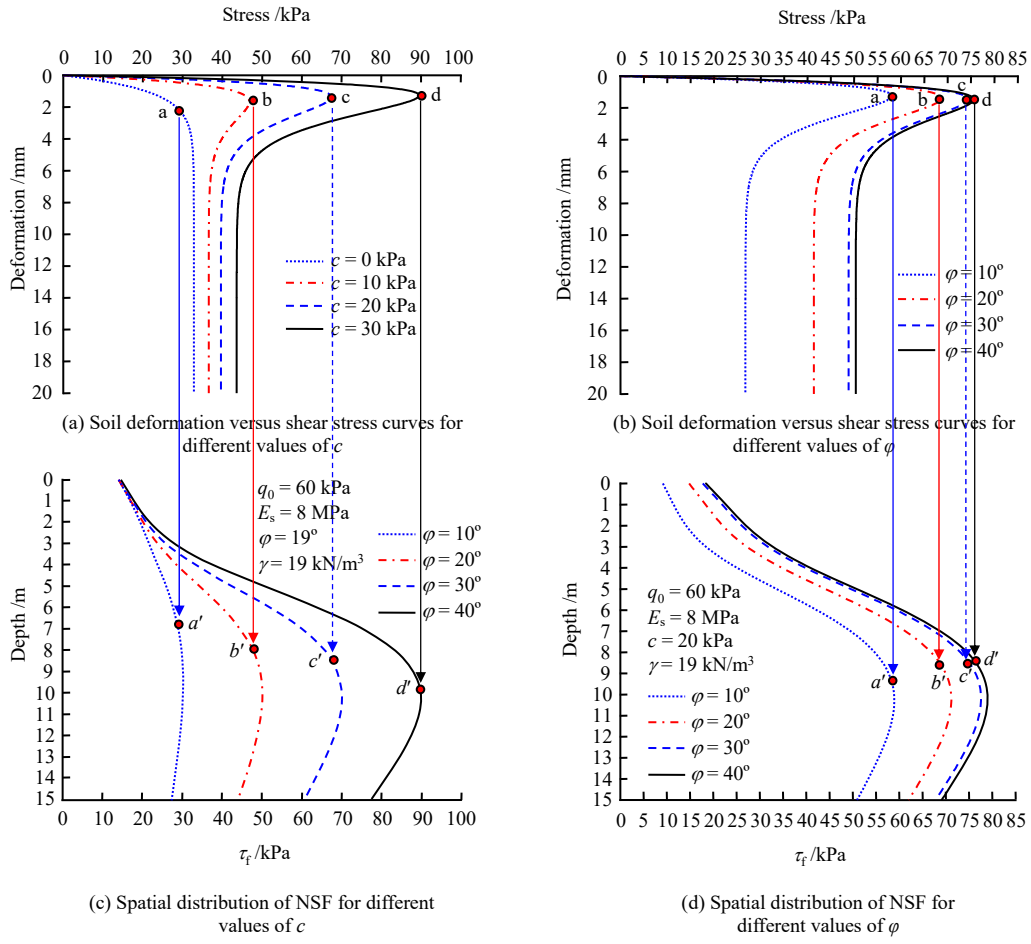


Fig. 9 The influence of different soil parameters on the spatial distribution of negative skin friction

in the internal friction angle.

4 Example verification

4.1 Project profile

The field test[41−42] is based on a converter station project in southwest Yunnan Province, which is located in a hilly and low mountain landform area. The test piles are bored piles with a borehole diameter of 800 mm and a length of 31 m. No external force on top of the pile, and the bedrock-embedded section of the piles ranges from 27 to 31 m. The test piles were designed with a diameter of 800 mm. The experiment monitored the soil settlement on the side of the pile and the axial force of the pile body and obtained the neutral point at 10 m of the pile body. The experiment monitored the soil settlement at the pile side and the axial force of the pile body and concluded that the neutral point was at 10 m of the pile body. The basic physico-mechanical parameters of the soil at the pile side and pile end are shown in Table 1. The layered settlement of the soil around the pile is shown in Fig. 10.

Table 1 The basic physical-mechanical parameters of soils

Soil name	Thicknesses /m	Weight /(kN • m^{-3})	Void ratio	Moisture content /%	Compression modulus /MPa	Cohesion /kPa	Frictional angle /(°)	Standard penetration test blow count $N_{63.5}$
Artificially filled soil	10.0	21.6	1.123	33.4	4.75	9.5	14	—
Quaternary clay layer	0.8−9.2	17.9	1.002	32.5	4.40	19.4	42	12.8
Silty clay	0.5−21.3	18.5	0.832	26.1	10.50	20.9	45	16.4
Limestone	—	27.2	—	—	—	—	—	—

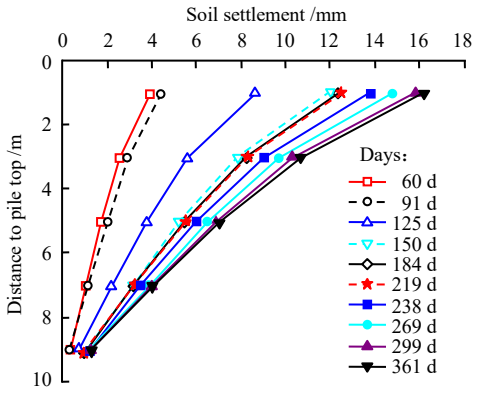


Fig. 10 Layered settlement of soil around piles

4.2 Calculation and Comparison

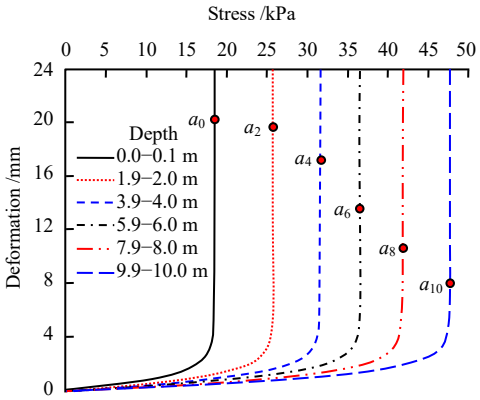
(1) Based on the relationship curve between pile side resistance and soil layer settlement, the values of ζ, λ, κ and χ of four parameters were determined according to the hyperbolic mechanical model. Specific values of the parameters (ζ, λ, κ, χ) were obtained and are shown in Table 2.

Table 2 Hyperbolic Mechanics Model Parameters

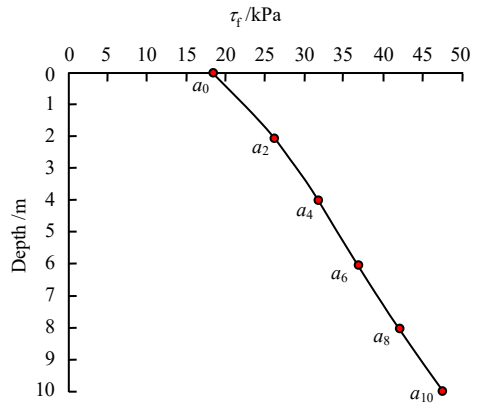
Soil	c /kPa	φ /(°)	λ	κ	ζ	χ
Artificially filled soil	9.5	14	1.1	−1.0	1 000.7	0.8

(2) Based on the field measurement of soil deformation around the pile, the soil is divided into n layers, each layer thickness is 100 mm. The strain of each soil layer is then calculated according to the method present in this paper.

(3) Based on the obtained hyperbolic mechanical model parameters and soil strains, the NSF of the pile body is derived according to the calculation method in this paper, see Fig. 11.



(a) Soil deformation and shear stress relationship curve at different depths



(b) NSF distribution curve

Fig. 11 NSF calculation result graphs

(4) Compare this with the NSF calculation method in

the *Chinese Technical Code for Building Pile Foundations* (JGJ 94—2008)[36], which has the following formula for NSF calculation:

$$\tau_{\mathrm{f}} = \beta\sigma'_{\mathrm{v}} \tag{15}$$

Where β is the negative skin friction coefficient and σ'_{v} is the vertical effective stress. β was 0.4 and 0.5, respectively, to calculate the NSF. The resulting curves are shown in Fig. 12.

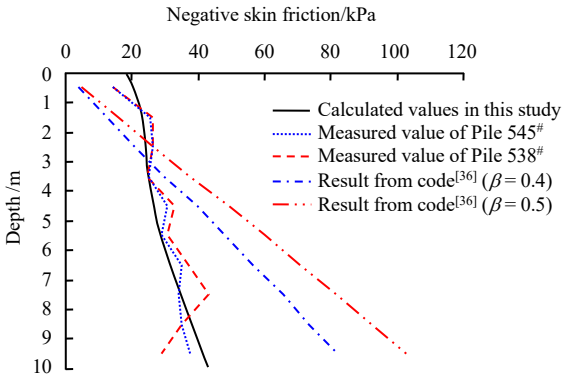


Fig. 12 Negative skin friction contrast curves

As shown from Fig. 11(a), the entire pile-soil contact surface is in the post-failure zone stress state, and the peak stress is close to the residual stress. This is consistent with the measured shear stress-deformation relationship in the field. Fig. 11(b) shows the distribution curve of NSF calculated by the method of this study.

Fig. 12 shows that the NSF calculated by the method in this paper is consistent with the measured values of #545 pile and #538 pile. The NSF calculated by Eq. (16) is similar to the measured NSF from 2 m to 4 m. Still, the difference between 4 m and the estimated value gradually increases, and the difference is three times at 10 m.

The drag loads obtained by the above methods are compared as shown in Table 3. It can be seen that the calculated value in this paper increases by 3.40% relative to the measured value of #538 and 7.75% relative to the measured value of #545 pile. This shows that the calculated values are close to the measured values and are safe and reliable. However, the computed values when β is taken as 0.4 and 0.5 in the code increased by 44.46% and 50.53% compared with the measured values of #538 and increased by 80.57% and 88.16% compared with the measured values of #545 pile, respectively. This indicates that the design of pile foundations according to the method in code will cause more significant economic loss. In contrast, the design of pile foundations with NSF obtained by the calculation method in this paper can be more economical. The difference between the calculated NSF in this study and the measured NSF is slight and straightforward, which can provide a reference for calculating NSF of pile foundations on engineering.

Table 3 The calculation result of drag load Q_n

Calculation Method	Q_n/kN	$\frac{Q_n - Q_1}{Q_1}$ /%	$\frac{Q_n - Q_2}{Q_2}$ /%
Measured value of pile #538 Q_1	716.15	0	—
Measured value of pile #545 Q_2	687.28	—	0
Result from code (β = 0.4) Q_3	1 034.54	44.46	50.53
Result from code (β = 0.5) Q_4	1 293.18	80.57	88.16
Calculated values in this study Q_5	740.53	3.40	7.75

5 Conclusions

A new method is proposed to calculate the negative skin friction (NSF) of piles under axially uniformly distributed loads by considering the complete stress state change during soil deformation and using a hyperbolic mechanical model to describe the stress-deformation relationship on the pile-soil contact surface. The effects of the degree of soil failure and changes in soil parameters on the spatial distribution of NSF were investigated, and the following conclusions were drawn:

(1) The stress state at the pile-soil contact surface during soil deformation can be divided into four stages: pre-failure zone, peak stress, post-failure zone, and residual stress. When the entire contact surface is in the pre-failure zone, the NSF increases slowly and then decreases rapidly along the pile. If the whole contact surface is partly in the pre-failure zone, partly in the peak stress, and partly in the post-failure zone and residual stress state, the NSF along the pile will increase slowly, then rapidly, and finally decrease slowly. If the entire contact surface is in the post-failure zone and residual stress state, the NSF increases slowly, decreases gradually, and increases rapidly along the pile.

(2) Increasing the soil cohesion will increase the extent of the contact surface in the post-failure zone stress state, and increasing the internal friction angle of the soil will reduce the extent of the contact surface in the post-failure zone stress state. Increasing soil cohesion changes the distribution characteristics of NSF, i.e., it increases the rate of change of NSF. However, increasing the angle of internal friction of the soil does not change the distribution characteristics of NSF; it will only increase the NSF in a linear relationship.

(3) All parameters involved in the calculation methods in this paper can be obtained directly from field or laboratory tests, which provides a higher degree of confidence than the normative methods. By comparing it with the field test results, the method of this paper is close to the measured values, which can provide a theoretical basis for the prediction of NSF during the design of pile foundations.

References

[1] CHIOU J, WEI W. Numerical investigation of pile-head load effects on the negative skin friction development of a

single pile in consolidating ground[J]. Acta Geotechnica, 2021, 16(6): 1867−1878.

[2] SEN T K, YAN W M, SE D. Fully coupled consolidation analysis of shear strength mobilization and dragload of a pile subject to negative skin friction[J]. International Journal of Geomechanics, 2015, 15(3): 04014057.

[3] HONG Y, NG C W W, CHEN Y M, et al. Field study of downdrag and dragload of bored piles in consolidating ground[J]. Journal of Performance of Constructed Facilities, 2016, 3(30): 4015050.

[4] XING H, LIU L. Field tests on influencing factors of negative skin friction for pile foundations in collapsible loess regions[J]. International Journal of Civil Engineering, 2018, 16(10B): 1413−1422.

[5] YANG Yong, DAI Zi-hang. Monitoring negative skin frictions on PHC pipe piles using FBG sensors[J]. Chinese Journal of Rock Mechanics and Engineering, 2017, 36(12): 3111−3120.

[6] WEI S T, LI B, YU J F, et al. Research on bearing capacity of piles with negative skin friction based on field test[C]// IOP Conference Series: Earth and Environmental Science. [S. l.]: [s. n.], 2024.

[7] WANG J, WU X, QIN W, et al. Negative skin friction of piles installed in dredged slurry after being reinforced by the vacuum preloading method[J]. Acta Geotechnica, 2023, 18(11): 6159−6174.

[8] SHI C C, YAN Y Y, DAI G L, et al. Experimental study of negative skin friction of pile group foundations for offshore wind turbines on artificial islands[J]. Journal of Marine Science and Engineering, 2024(12): 1386.

[9] LIU Y, YANG P, XUE S, et al. Influence of dredger fill self-consolidation on development of negative skin friction of piles[J]. Arabian Journal of Geosciences, 2020, 13(15): 725.

[10] ZHAO Z, YE S, ZHU Y, et al. Scale model test study on negative skin friction of piles considering the collapsibility of loess[J]. Acta Geotechnica, 2022, 17(2): 601−611.

[11] TERZAGHI K, PECK R. Soil mechanics in engineering practice[M]. New York: Wiley, 1948.

[12] KONG G Q, ZHOU H, LIU H L, et al. A simplified approach for negative skin friction calculation of special-shaped pile considering pile-soil interaction under surcharge[J]. Jurnal of Central South University, 2014, 21(9): 3648−3655.

[13] ZHAO Ming-hua, HE Wei, CAO Wen-gui. Study on calculation of negative skin friction resistance on piles[J]. Rock and Soil Mechanics, 2004, 25(9): 1442−1446.

[14] ZHAO Ming-hua, LIU Si-si. Numerical simulation of negative skin friction on single pile in multiple layer deposits[J]. Chinese Journal of Geotechnical Engineering, 2008, 30(3): 336−340.

[15] SEED H B, REESE L C. The action of soft clay along friction piles[J]. ASCE Soil Mechanics and Foundation Division Journal, 1957, 122(1): 731−754.

[16] CAO W, CHEN Y, WOLFE W E. New load transfer hyperbolic model for pile-soil interface and negative skin friction on single piles embedded in soft soils[J]. International Journal of Geomechanics, 2014, 14(1): 92−100.

[17] CHEN R P, ZHOU W H, CHEN Y M. Influences of soil consolidation and pile load on the development of negative skin friction of a pile[J]. Computers and Geotechnics, 2009, 36(8): 1265−1271.

[18] KIM H J, MISSION J L, PARK T W, et al. Analysis of negative skin friction on single piles by one dimensional consolidation model test[J]. International Journal of Civil Engineering, 2018, 16(10B): 1445−1461.

[19] ZHANF Y, WU W, JIANG G, et al. A new approach for estimating the vertical elastic settlement of a single pile based on the fictitious soil pile model[J]. Computers and Geotechnics, 2021, 134: 104100.

[20] SHAO L, WANG H, LI H, et al. Criterion of shear failure along a surface inside soil-mass and its application to progressive failure analysis[J]. Bulletin of Engineering Geology and the Environment, 2023, 82(7): 244.

[21] GAN Fei, YE Xiao-ming, YING Ke, et al. Experimental Study on progressive failure of soil-structure interfaces based on a new measuring method of local stress and displacement[J]. Chinese Journal of Rock Mechanics and Engineering, 2018, 37(3): 734−742.

[22] SHAO L T, LIU G, ZENG F T, et al. Recognition of the stress–strain curve based on the local deformation measurement of soil specimens in the triaxial test[J]. Geotechnical Testing Journal, 2016, 39(4): 20140273.

[23] LI X, VANAPALLI S K. Simulation of progressive shear failure in railway foundation[J]. Transportation Geotechnics, 2021, 29: 100500.

[24] WU Y, REN Y, LIU J, et al. Analysis of negative skin friction on a single pile based on the effective stress method and the finite element method[J]. Applied Sciences-Basel, 2022, 12(9): 4125.

[25] GAN Fei, YE Xiao-ming, ZHENG Gang, et al. A new type of shear stress model-hyperbolic mechanical model[J]. Chinese Journal of Rock Mechanics and Engineering, 2021, 40(Suppl.2): 3253−3260.

[26] GAN Fei. The hyperbolic progressive shear- failure mode of soil and its application in stability analysis of landslide[D]. Chongqing: Chongqing University, 2017.

[27] CAO F, YE C, WU Z, et al. Settlement calculation of semi-rigid pile composite foundation on ultra-soft soil under embankment load[J]. Buildings, 2024, 7(14): 1954.

[28] DAVIS E H, POULOS H G. The settlement behaviour of single axially loaded incompressible piles and piers[J]. Géotechnique, 1968, 18(3): 351−371.

[29] LI S, LI P, ZHANG M. Analysis of additional stress for a curved shield tunnel[J]. Tunnelling and Underground Space Technology, 2021, 107: 103675.

[30] HE Cheng-bin, ZHAO Ming-hua, LEI-Yong. Negative friction computational research of rock-socketed pile based on load transfer method[J]. Engineering Mechanics, 2014, 31(11): 110−115.

[31] ABDRABBO F M, ALI N A. Behaviour of single pile in consolidating soil[J]. Alexandria Engineering Journal, 2015, 54(3): 481−495.

[32] WU W, WANG Z, ZHANG Y, et al. Semi-analytical solution for negative skin friction development on deep foundations in coastal reclamation areas[J]. International Journal of Mechanical Sciences, 2023, 241: 107981.

[33] JIANG Gang, ZAI Jin-min, CHEN Guo-xing, et al. Design of composite pile foundation and settlement calculation[J]. Rock and Soil Mechanics, 2003, 24(3): 405−409.

[34] YU J, CHEN J, ZHOU J, et al. Analytical modeling for the behavior of concrete-cored cement mixing (CCM) pile composite foundation under embankment[J]. Computers and Geotechnics, 2024, 167: 106084.

[35] ZHAO Ming-hua. Soil mechanics and foundation engineering[M]. Wuhan: Wuhan University of Technology Press, 2009.

[36] Ministry of Housing and Urban-Rural Development of the People's Republic of China. JGJ94−2008. Technical code for building pile foundations[S]. Beijing: China Architecture & Building Press, 2008.

[37] LIU Zi-sheng. Field tests on negative skin friction of steel pipe piles in high backfilling soils[J]. Chinese Journal of Geotechnical Engineering, 2015, 37(2): 337−342.

[38] MASHHOUR I, HANNA A. Drag load on end-bearing piles in collapsible soil due to inundation[J]. Canadian Geotechnical Journal, 2016, 53(12): 2030−2038.

[39] CHEN Jing, LI Shao-jun, MENG Fan-zhen, et al. Experimental study of mechanical properties of interface between pile and macadam soil in accumulative landslide in the Three Gorges Reservoir Area[J]. Chinese Journal of Rock Mechanics and Engineering, 2011, 30(Suppl.1): 2888−2895.

[40] LIU H Y, ZHU M X, LI X J, et al. Experimental study on shear behavior of interface between different soil materials and concrete under variable normal stress[J]. Applied Science-Basel. 2022, 12: 11213.

[41] WU Shuang-shuang, HU Xin-li, GONG Hui, et al. Shear properties of pile-soil of three modes of bored piles in field tests[J]. Rock and Soil Mechanics, 2019, 40(7): 2838−2846.

[42] WU Shuang-shuang, HU Xin-li, ZHANG Han, et al. Field test and calculation method of negative skin friction of rock-socketed piles[J]. Rock and Soil Mechanics, 2019, 40(9): 3610−3617.